Available online at www.sciencedirect.com
ScienceDirect
International Journal of Thermal Sciences 47 (2008) 1306–1315
International Journal of Thermal Sciences
www.elsevier.com/locate/ijts

The thermal modeling of a matrix heat exchanger using a porous medium and the thermal non-equilibrium model

Andrew M. Hayes [a,b,*], Jamil A. Khan [a], Aly H. Shaaban [b], Ian G. Spearing [c]

[a] *University of South Carolina, Columbia, SC, USA*
[b] *Applied Research Associates, Inc., Panama City, FL, USA*
[c] *Liebert Corporation, Columbus, OH, USA*

Received 24 April 2007; received in revised form 5 November 2007; accepted 5 November 2007

Available online 21 February 2008

Abstract

Heat transfer and fluid flow characteristics through a porous medium were investigated using numerical simulations and experiment. For the numerical simulations two models were created: a two-dimensional numerical model and a Fluent™ computational fluid dynamics (CFD) porous media model. The experimental investigation consisted of a flow channel with a porous medium section that was heated from below by a heat source. The results of the numerical models were compared to the experimental data in order to determine the accuracy of the models. The numerical model was then modified to better simulate a matrix heat exchanger. This numerical model then generated temperature profiles that were used to calculate the heat transfer coefficient of the matrix heat exchanger and develop a correlation between the Nusselt number and the Reynolds number.

Keywords: Porous media; Matrix heat exchanger; Heat transfer; Thermal non-equilibrium; Thermal modeling

1. Introduction

During the pursuit of compact heat exchangers that are able to perform in demanding circumstances a series of stacked plate-spacer pairs was developed to exchange heat between multiple streams. This micro-heat exchanger is called a matrix heat exchanger. The plates are made of a highly thermally conductive material and are used to transfer the heat between the fluid streams. The spacers are made of less thermally conductive material and are used to inhibit axial conduction and enable flow re-distribution. Fig. 1 is a schematic of a matrix heat exchanger, from now on referred to as MHE.

When the fluid passes through the holes of the perforated plate heat is exchanged between the plate and the fluid. The perforated plate surface area consists of the front and back of the plate as well as the (inner) wall surface area of each perforation. The large surface area of each sheet gives the matrix heat exchanger a large surface area to volume ratio, thus enabling compact exchangers with high heat transfer rates.

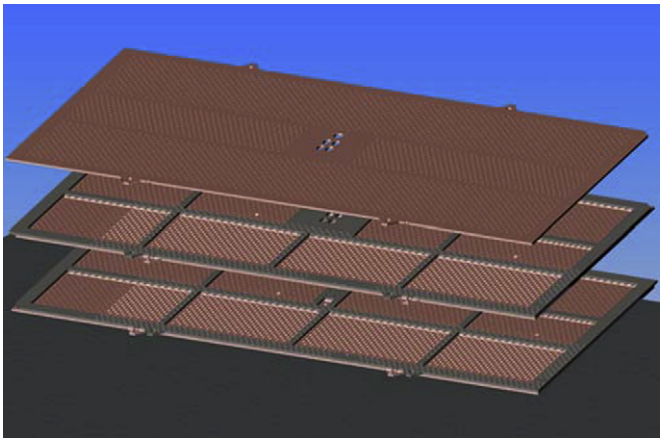

Fig. 1.

The flow characteristics through an MHE have been studied by numerous researchers. Many of the researchers have stud-

* Corresponding author.
E-mail address: mettler@aol.com (A.M. Hayes).

1290-0729/$ – see front matter
doi:10.1016/j.ijthermalsci.2007.11.005

Nomenclature

Da	Darcy number	m^{-2}
C_p	fluid specific heat	J/kg K
d	diameter	m
F	inertia coefficient (dimensionless)	
G	mass flow rate	kg/s
h	heat transfer coefficient	W/m^2 K
h_v	volumetric heat transfer coefficient	W/m^2 K
K	permeability	m^2
L	length	m
M	mass flux rate	kg/m^2 s
Nu	Nusselt number	
P^*	dimensionless pressure	
Pr	Prandtl number	
q	heat flux	W/m^2
Re	Reynolds number	
T	temperature	K
u	velocity	m/s
U	dimensionless velocity	
V	velocity	m/s
$\|V\|$	velocity magnitude $\sqrt{u_x^2+u_y^2}$	
W	channel width	m
X	dimensionless length	
Y	dimensionless height	

Greek symbols

δ	plate thickness	m
ε	porosity	
λ	thermal conductivity	W/m K
η	efficiency	
ρ	fluid density	kg/m^3
ϑ	dimensionless temperature	
ψ	stream function	
μ	fluid viscosity	$N s/m^2$

Subscripts

D	Darcian
d	dispersion
f	fluid
m	mean
p	particle
s	solid
tc	distance from heated surface to thermocouple
v	volumetric
w	wall
x	x-direction
y	y-direction

ied flow through one perforated plate in hopes to be able to model the data into a corresponding relationship between flow characteristics and heat transfer. Sparrow et al. [1] was able to derive an average Nusselt number correlation as a function of the Reynolds number and Prandtl number. From that correlation the average convective heat transfer coefficient for the plate was determined based on the Reynolds number of the perforated plate's hole. Cho et al. [2] performed laboratory experiments using the naphthalene sublimation technique to determine the heat transfer coefficient characteristics of a short hole in a plate. The experiments examined hole-length-to-diameter ratios of 0.5–1.5 and outer-boundary-to-hole of 1.4–4.5. The hole diameters were 12.6–38.1 mm, and the Reynolds number varied from 100 to 30,000. The results were broken into three sections: windward face, inside the hole, and leeward face. Gong et al. [3] studied how the hole-length-to-diameter ratio of the plate affected the heat transfer coefficient of a perforated plate. They studied ratios varying from 0.333 to 1.1666. They held the diameter constant while the thickness was varied. Brunger et al. [4], studied the effectiveness for each of the three zones of heat transfer on a perforated plate: the front of the plate, inside the tube, and the back of the plate. In their study the pitch to diameter ratio was quite large (>6.67). Imke [5] developed a numerical model to simulate micro-channel flow and heat transfer in compact heat exchangers based on the forced convection porous body approach. Boomsma et al. [6], experimented on the thermal performance of aluminum metal foams. Experiments were conducted to determine the pressure drop and the heat exchanger performance. Applications that incorporate the perforated plate are the making of fiberglass threads, the upstream tube sheet of a shell and tube heat exchanger, and devices that smooth non-uniform flow [2]. Perforated sheets have also been widely used in the heating of air for building/office-space air conditioning.

Venkatarathnam and Sarangi [7] and Venkatarathnam [8] studied characteristics of heat transfer and fluid flow through actual MHEs. Venkatarathnam [8] then proceeded to solve numerical models in which to compare actual laboratory results. Through his numerical solutions he was able to derive number of transfer units (NTU) relationships, and Nusselt–Reynolds correlations for the MHE. He was also able to derive a system in which to size the matrix heat exchangers based on fluid properties and operating conditions.

Researchers have also studied the flow characteristics and have added terms to the governing fluid flow equations in order to facilitate the modeling of the conditions that the fluid encounters as it flows through porous media. The Brinkman extension and Forchheimer extension are typical additions. Also, when modeling the heat transfer in porous media, researchers have derived many different boundary conditions for the numerical model [9–11].

Over the last two decades there has been an increased amount of research into the use of porous media for the purpose of enhancing the heat transfer rates. Porous media heat exchangers (PMHE) offer a large amount heat transfer to occur within a small volume. The local thermal equilibrium model (LTE) is widely used to solve the heat transfer characteristics. This model assumes that the fluid temperature and porous me-

dia temperature are the same at any point in the porous media. As opposed to the local thermal equilibrium model (LTE), the local thermal non-equilibrium model (LTNE) assumes a finite difference between the fluid and the porous media and solves for their respective temperatures separately. The LTNE model has two equations describing the heat transfer within the porous media. One equation is accounting for the heat transfer due to the fluid's convection, while the other equation is accounting for the heat transfer due to conduction within the porous media.

Research has been done on the LTNE model's application to PMHE. Pavel and Mohamad [12] examined the influence that different diameter porous media had on the Nusselt number. Alazmi and Vafai [13] studied how different boundary conditions can affect the heat transfer model. Different parameters such as the porosity, Darcy number, Reynolds number, inertia parameter, particle diameter, and solid-to-fluid conductivity ratio were analyzed. Jiang et al. [10] went over an in depth numerical model of heat transfer in a channel packed with various materials: glass, stainless steel, and bronze. The numerical model's output was compared with experimental data for verification. The authors tested various boundary conditions that incorporated the thermal properties of the fluid and the porous media as well as the porosity and settled on the ideal constant wall heat flux boundary condition. Also discussed were the effects of viscous dissipation on the heat transfer coefficient. It was found that for most practical uses the effects of viscous dissipation can be ignored. Zhang and Huang [14] used the volume averaging method (VAM) to develop a volumetric heat transfer coefficient (VHTC) model. The paper outlined the mathematical approach using a closure variable then went through a solution procedure with periodic boundary conditions. Jeng et al. [15], Whitaker [16] and Khashan et al. [17] set forth conditions in which the use LTNE model is validated. These conditions were based on volumetric heat transfer coefficient, the temperature difference between the fluid and the solid, the length scale ratio, the difference between the thermal properties of the fluid and solid, and the porosities.

The present paper investigates the local thermal equilibrium model used by Fluent™ and the local thermal non-equilibrium model in relationship to the thermal modeling of heat transfer in a porous medium. The study was used to determine which model better represents the thermal aspects of the porous medium, and consisted of a physical model, an in-house developed numerical model, and a Fluent™ porous media model. Next, a correlation between the Nusselt number and Reynolds number was developed for the porous medium heat exchanger from the data collected. This correlation was then compared to developed correlations from earlier studies and from other author's studies for a matrix heat exchanger.

2. Two-dimensional flow model for porous media

The steady-state two-dimensional governing equations for single phase fluid flow in an isotropic, homogenous, porous media based on the Brinkman–Darcy–Forchheimer model with constant properties can be written as: [1,13]

$$\frac{\rho}{\varepsilon^2}(V\cdot\nabla)V = -\nabla P - \frac{\mu}{K}V + \frac{F\rho}{\sqrt{K}}|V|V + \frac{\mu}{\varepsilon}\nabla^2 V \tag{1}$$

The fluid velocities in terms of the stream-function are:

$$u_x = \frac{\partial\psi}{\partial y} \tag{2}$$

and

$$u_y = \frac{-\partial\psi}{\partial x} \tag{3}$$

Non-dimensionalizing yields for the x-direction:

$$U_x\frac{\partial U_x}{\partial X} + U_y\frac{\partial U_x}{\partial Y} = -\frac{\varepsilon^2}{\rho}\frac{\partial P^*}{\partial X} - \frac{\varepsilon^2}{Re\,Da}U_x + \frac{F\varepsilon^2}{\sqrt{Da}}|V|U_x + \frac{\varepsilon}{Re}\left(\frac{\partial^2 U_x}{\partial X^2} + \frac{\partial^2 U_x}{\partial Y^2}\right) \tag{4}$$

And the y-direction:

$$U_x\frac{\partial U_y}{\partial X} + U_y\frac{\partial U_y}{\partial Y} = -\frac{\varepsilon^2}{\rho}\frac{\partial P^*}{\partial Y} - \frac{\varepsilon^2}{Re\,Da}U_y + \frac{F\varepsilon^2}{\sqrt{Da}}|V|U_y + \frac{\varepsilon}{Re}\left(\frac{\partial^2 U_y}{\partial X^2} + \frac{\partial^2 U_y}{\partial Y^2}\right) \tag{5}$$

Taking the curl of the x-direction (4) and y-direction (5) momentum equation, inserting Eqs. (2) and (3) and re-arranging gives the flow through porous media as:

$$\frac{\varepsilon}{Da}\left(\nabla^2\psi\right) + \nabla^4\psi = \frac{Re}{\varepsilon}U_x\left[\left(\frac{\partial^3\psi}{\partial X^3}\right) + \left(\frac{\partial^3\psi}{\partial Y^2\partial X}\right)\right] + \frac{Re}{\varepsilon}U_y\left[\left(\frac{\partial^3\psi}{\partial X^2\partial Y}\right) + \left(\frac{\partial^3\psi}{\partial Y^3}\right)\right] \tag{6}$$

Eq. (6) represents the stream function-velocity model for flow through porous media. (Eq. (6) was solved by an iterative approach similar to that used by Gupta et al. [18] until a convergence criterion of $\frac{U_x^{n+1}-U_x^n}{U_x^n} \leqslant .5E{-}06$; in which n was the nth iteration, was satisfied.)

In order to solve Eq. (6) it was necessary to obtain the permeability, K, and inertia coefficient, F. The Forchheimer equation was used to obtain these values:

$$\Delta p = \frac{\mu L}{K}V_D + \frac{\rho F L}{\sqrt{K}}V_D^2 \tag{7}$$

By substituting $C_1 = \mu L/K$ and $C_2 = \rho F L/\sqrt{K}$, Eq. (5) can be rewritten as:

$$\Delta p = C_1 V_D + C_2 V_D^2 \tag{8}$$

C_1 and C_2 in Eq. (8) were determined by a second order polynomial curve fit to the measured pressure drop across the porous media for different Darcian velocities. As a result of knowing C_1 and C_2, it was possible to obtain the coefficients K and F.

3. In-house model for energy equation

The numerical model was based on Jiang et al.'s [9], work in the thermal development of flow through porous media. Fluid velocities obtained from the solution of Eq. (6) were used in the numerical heat transfer model to obtain the temperature profiles in the porous medium.

The fluid-phase and solid-phase energy equations for the thermal non-equilibrium model with consideration of thermal dispersion, viscous dissipation, constant porosity and constant properties are as follows. For the fluid phase:

$$\rho_f c_{pf}\varepsilon\left[u_x\frac{\partial(T_f)}{\partial x}+u_y\frac{\partial(T_f)}{\partial y}\right] = \frac{\partial}{\partial y}(\varepsilon\lambda_f+\lambda_d)\left[\frac{\partial T_f}{\partial y}\right]+\frac{\varepsilon\mu_f}{K}u_x^2 + \varepsilon^2\frac{\rho_f F}{\sqrt{K}}|V|u_x^2+\frac{h_v}{\varepsilon}(T_s-T_f) \tag{9}$$

With viscous dissipation being defined as *the rate at which mechanical energy is irreversibly converted to thermal energy due to viscous effects in the fluid* [19], and due to the amount of surface area in contact with the fluid as it moves through a porous media one can see that the work required to keep the fluid in motion increases substantially.

And for the solid phase:

$$(1-\varepsilon)\frac{\partial}{\partial y}\left[\lambda_s\frac{\partial T_s}{\partial y}\right]-\frac{h_v}{\varepsilon}(T_s-T_f)=0 \tag{10}$$

Non-dimensionalizing (7) yielded:

$$U_x\frac{\partial(\theta_f)}{\partial X}+U_y\frac{\partial(\theta_f)}{\partial Y}=\frac{1}{\varepsilon\,Re\,Pr}\left[\frac{\partial}{\partial Y}\left(\frac{\varepsilon\lambda_f+\lambda_d}{\lambda_f}\right)\frac{\partial\theta_f}{\partial Y}\right] + \frac{1}{Da\,Re}\frac{U_{\text{in}}^2\varepsilon\lambda_f}{c_{pf}q_wH}\left(U_x^2\right)+\frac{U_{\text{in}}^2F\varepsilon^2\lambda_f}{c_{pf}q_wH\sqrt{Da}}|V|U_x^2 + \frac{Nu_{sf}}{Re\,Pr}\left[\frac{\partial^2\theta}{\partial Y^2}\right] \tag{11}$$

And (8) yielded:

$$(1-\varepsilon)\frac{\lambda_s}{\lambda_f}\left[\frac{\partial^2\vartheta_s}{\partial Y^2}\right]-Nu_{sf}(\vartheta_s-\vartheta_f)=0 \tag{12}$$

The equations were discretized and then solved using the implicit finite-element method.

The boundary conditions for the thermal non-equilibrium model were those mentioned by Jiang et al. [9] and Alazmi and Vafai [13]. Following Jiang et al. [9], there are four different methods for treating the boundary interface of the porous media and the fluid. As mentioned earlier, the thermal non-equilibrium model assumes that the temperature of the fluid and the temperature of the porous media are different at this interface.

$$q_w=-\lambda_{fw}\left(\frac{\partial T_f}{\partial y}\right)_w=-\lambda_s\left(\frac{\partial T_s}{\partial y}\right)_w \tag{13}$$

Although the fluid and solid temperature may be very close at the wall, Jiang et al. [9] showed that Eq. (13) was best for modeling heat transfer in porous media. As a result, Eq. (13) was used as the boundary condition on the heated wall.

The Reynolds number could be represented by the following correlations given by Jiang et al. [9], Alazmi and Vafai [13], and Boomsma et al. [6].

The final equation for the Reynolds number used in this research was

$$Re=\frac{2Md_p}{3\mu(1-\varepsilon)} \tag{14}$$

The local heat transfer coefficient was calculated as:

$$h_x=\frac{q_w}{(T_{wx}-T_{\text{in}})} \tag{15}$$

And the local Nusselt number as

$$Nu_x=\frac{h_xD_h}{\lambda_f} \tag{16}$$

While the mean heat transfer coefficient and Nusselt number were calculated using the average wall temperature and fluid temperature as follows

$$h_m=\frac{q_w}{(T_{wm}-T_{fm})} \tag{17}$$

$$Nu_m=\frac{h_mD_h}{\lambda_{fm}} \tag{18}$$

with

$$D_h=\frac{2hW}{(h+W)} \tag{19}$$

The average wall temperature, T_{wm}, was the average of the thermocouple readings at the wall, while the mean fluid temperature, T_{fm}, was the average of the inlet and outlet fluid temperatures. The local temperature of the heat transfer surface was calculated using the measured temperatures of the wall.

$$T_{wx}=T_x-\frac{q_w\delta_{tc}}{\lambda_s} \tag{20}$$

The local bulk fluid temperature was defined as:

$$T_{fb}=T_{\text{in}}+\frac{q_w}{Gc_p}Wx \tag{21}$$

Jiang [9] presented a modified thermal dispersion equation that matched his experimental data well:

$$\lambda_d=C(\rho c_p)_f d_p\sqrt{u_{xp}^2+u_{yp}^2}(1-\varepsilon) \tag{22}$$

with

$$C=1.042\left(\rho_f c_{pf}d_pu_{xp}(1-\varepsilon_m)\right)_{\text{in}}^{-0.8282} \tag{23}$$

The above equations were used in the in-house numerical model and compared to the data obtained from the laboratory experiments and to the output from the Fluent™ model.

4. Boundary conditions for numerical solution

The no-slip boundary condition and no-penetration at the wall boundary condition were defined for the numerical model, along with the following.

At $X=0$: $U_{\text{in}}=\text{constant}$, $U_y=0$; $\psi_{0,j}=jU_{\text{in}}\Delta y$

In which j is the y-direction distance from $y=0$

$$\text{At } X = 1: \quad \frac{\partial U_x}{\partial X} = 0;\ \frac{\partial U_y}{\partial Y} = 0;\ \frac{\partial \psi}{\partial X} = 0;\ \frac{\partial \psi}{\partial Y} = 0$$
$$\text{At } Y = 0 \text{ and } Y = 1: \quad \psi = 0;\ U_x = 0;\ U_y = 0$$

In solving the equations for heat transfer in the porous medium an iteration method was used. The model assumed a constant wall heat flux. The method involved initial guesses for the temperatures, while the inertial coefficient and permeability were obtained from the laboratory experiment explained earlier, the volumetric heat transfer, h_v, was known, and the fluid velocities were known from the solution of Eq. (6). By first solving (9) for the last term on the RHS and subsequently using its solution to solve (10) for the $\frac{\partial T_s}{\partial y}$ expression it was possible to update the solid temperatures and then update the fluid temperatures.

5. Fluent™ model

Fluent™'s porous media model uses the thermal-equilibrium model to solve numerous problems such as: packed beds, flow through paper filters, perforated plates, and flow distributors. Heat transfer can be represented in the porous medium under the assumption of thermal equilibrium between the porous medium and the fluid. The porous media model in Fluent™ was a two-dimensional model consisting of a flow channel with a mid-section representing the porous medium. The dimensions of the Fluent™ model matched the dimensions of the physical model used in the laboratory experiments. The number of nodes in the Fluent™ model and the in-house numerical model were same: 240 in x-direction and 40 in the y-direction.

The porous media model contains settings for the following variables: the viscous resistance, the inertia resistance, and the porosity. The viscous resistance and the inertia resistance values were obtained from the experiment mentioned in Section 2.

After defining the terms it was necessary to define the fluid properties, the material properties of the porous medium, and the boundary conditions used in the solution.

The porous medium was modeled in Fluent™ with the addition of a source term to the momentum equation

$$S_i = -\left(\sum_{j=1}^{3} D_{ij}\mu V_{ij} + \sum_{j=1}^{3} C_{ij}\frac{1}{2}\rho|V|V_j\right) \tag{24}$$

For a simple homogenous porous media, Fluent™'s source term was

$$S_i = -\left(\frac{\mu}{K}V_i + F\frac{1}{2}\rho|V|V_i\right) \tag{25}$$

The first term on the right-hand side of Eq. (25) takes into consideration the permeability of the porous medium, K, while the second term takes into consideration the inertial resistance factor, F.

The thermal equilibrium energy equation used by Fluent for the solution was:

$$\frac{\partial}{\partial t}\left(\varepsilon\rho_f E_f + (1-\varepsilon)\rho_s E_s\right) + \nabla\cdot\left(\vec{v}(\rho_f E_f + P)\right) = \nabla\cdot\left[\lambda_{\text{eff}}\nabla T - \sum_i h_i J_i + (\tau\cdot\vec{v})\right] + S_f^h \tag{26}$$

The last term on the right-hand side of Eq. (26) is the enthalpy source term which defines any heat from chemical reactions or any other volumetric heat sources.

The effective thermal conductivity, λ_{eff}, of the porous medium was defined as

$$\lambda_{\text{eff}} = \varepsilon\lambda_f + (1-\varepsilon)\lambda_s \tag{27}$$

The boundary condition used by Fluent™ for the heat flux was:

$$q = h_f(T_s - T_f) \tag{28}$$

whereas, the fluid side heat transfer was calculated using

$$q_w = -\lambda_f\left(\frac{\partial T}{\partial y}\right)_w \tag{29}$$

The fluid flow model in Fluent™ was based on laminar flow. This meant that the generation of turbulence within the porous medium was zero and the effects on the momentum equation were also zero.

After defining the necessary boundary conditions and defining the physical attributes, the model was solved using Fluent™'s finite volume solver. For post processing Fluent™ was also used. The post processing involved the output files of velocity in the x- and y-direction, the heat input, and the temperatures. Each of the laboratory experiments were replicated in Fluent™. The data were collected and graphed for comparison.

6. Laboratory model

The physical model used in the experiments was very similar to the model used by Jiang et al. [10]. Fig. 2 is a representation of the experimental model. The experimental apparatus shown in Fig. 2, consisted of a water pump (1), a test section (2), a heater block (3), thermocouples (4), power source (5), data reader (6), data acquisition computer (7), and the porous medium test section (8).

The model assumes the porous medium was isotropic and homogeneous, and the fluid was single phase, with constant properties. The lower side of the porous medium received a constant heat input, q, while the upper side was adiabatic. The size of the heated test section was 38 mm × 38 mm. The flow en-

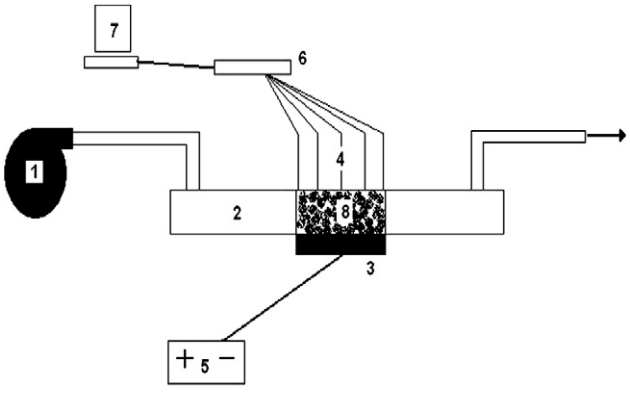

Fig. 2.

tered the channel with an average velocity, u_{in}, and constant temperature, T_{in}.

The test section was made from lexan, and consisted of an upper and lower section. The lower section contained the flow channel and section for the porous medium. The porous medium was obtained from ERG, Inc. and was constructed of aluminum 6101 with constant porosities and a thermal conductivity of 230 W/m K. Two different pore sizes were tested: a coarse sample at 10 PPI (pores per inch) and a fine sample at 40 PPI. The fiber diameter of the fine porosity piece was 0.0004 m and had a porosity of 0.925, while the diameter of the coarse porosity piece was 0.001 m and had a porosity of 0.9167. The dimensions of the porous medium were 0.0381 m × 0.0381 m × 0.0127 m.

The upper section also contained the inlet and outlet holes for the fluid as well as the thermocouple insertion points. The lower section contained the heater block. The heating block was constructed of aluminum which held two 120 V/20 W heaters. It was 38 mm × 38 mm × 19 mm thick. Each heater was a CSS-10120/120 V model that was 6.35 mm in diameter and 25.4 mm in length. A multi-voltage rheostat applied voltage to the heaters. The porous medium, after being installed in the lower test section, was compressed approximately 0.010″ after installing the upper section to insure conformity with the flow channel.

Four thermocouples were placed along the center line of the test section. They were inserted mid-way into the porous medium. The temperature of the fluid next to the wall was monitored along the upper corner with four thermocouples equally spaced. The fluid temperature next to the heater block was also monitored along the lower corner with four equally spaced thermocouples. The heat block's temperature was also monitored with a thermocouple. The inlet and outlet temperature of the fluid was measured with a thermocouple placed at the inlet region and exit region of the lexan test apparatus. Inlet pressure was monitored using a pressure transducer. The mass flow rate of the water was controlled by 3-piston pump from Eldex Laboratories, model BBB-4.

Water was used as the working fluid for the experiments. A typical test involved a specific flow rate, voltage input, and inlet fluid temperature. The test was conducted at incremental increases in voltage to the heaters.

The heat loss from the heated section to the adjacent section by conduction and to the atmosphere by radiation and convection was determined by a separate experiment similar to that done by Pavel and Mohamad [12]. Therefore, by knowing the heat loss at certain power inputs, adjustments were made to account for the losses in order to determine the overall power input into the porous medium.

7. Fluent™ porous media results

After determining the inertia and viscous terms it was possible to set the boundary conditions in Fluent™. Results were obtained for each of the separate velocities as well as separate inlet temperatures and heating input. Since the heat was applied only at the bottom wall, the temperature of the fluid was at the highest at the bottom of the porous medium and increased as the fluid traveled in the x-direction along the same plane. The temperature in y-direction along the same plane decreased as the distance from the bottom wall increased. Fig. 3 represents the resulting temperature contours of the porous medium section. The flow pattern, Fig. 4, as solved for by Fluent™, showed an initial section of flow re-adjustment due to the pressure jump experienced by the fluid as it entered the porous medium.

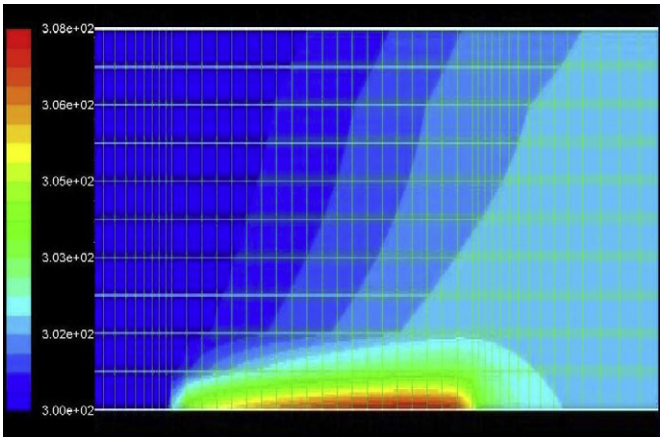

Fig. 3.

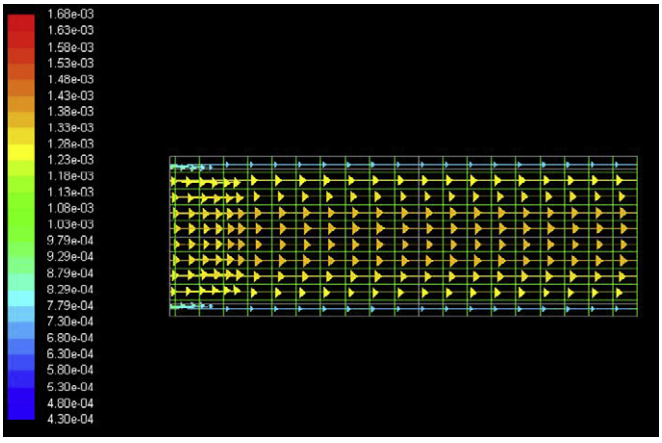

Fig. 4.

8. Two-dimensional numerical fluid flow results

The velocity profile of fluid flow through porous medium was similar to plug flow. This was due to channeling effects of the porous medium, and the constant porosity of the porous medium. The no slip boundary condition at the wall caused the steep velocity gradient at the wall [9]. Fig. 5 represents the flow field from the centerline to the wall traveling in the positive y-direction.

The entrance effects could not be captured in the numerical model. These were caused by the sudden change in flow conditions from open channel, uniform velocity to that of flow in porous medium. Jiang et al. [9] also discussed these effects as being difficult to numerically model.

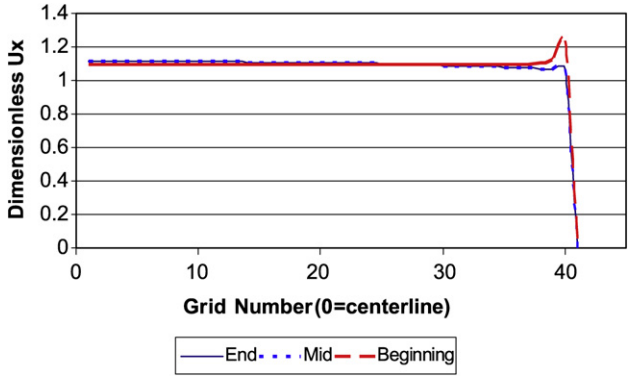

Fig. 5.

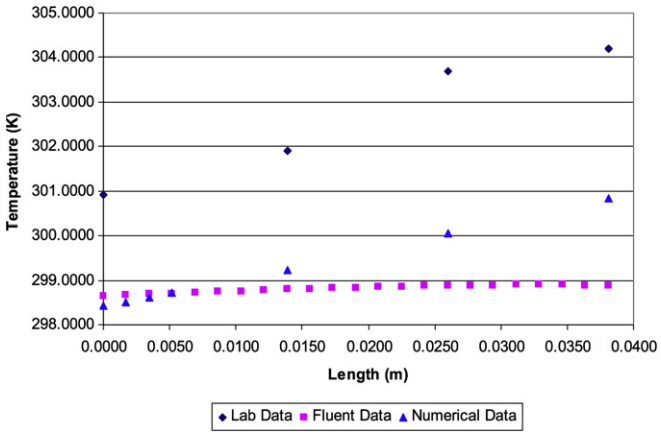

Fig. 6.

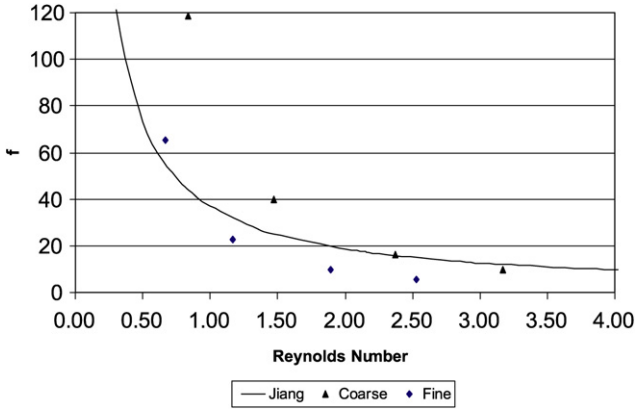

Fig. 7.

9. Laboratory and numerical results

The Kline–McClintock method for uncertainty was used to investigate the uncertainty in the heat transfer coefficient. This involved the uncertainty in the thermocouple reading, the uncertainty in the measurement of the area of the porous block, and the uncertainty in the voltage reading. Using these uncertainties the heat transfer coefficient had an error of 2.7%.

The computational domain used in the numerical model was rectangular in shape, with the length equal to 6 times the height. Five different grid sizes were checked to determine the effects on the temperature field. The average of the final column of temperatures, T_{out}, checked against each other for each of the numerical solutions. A vertical grid count of 25, 30, 35, 40, and 45 was examined. The percent difference between each of the final temperatures decreased as the grid size increased. The differences between 35 and 40 was less than 1.7×10^{-6}, while the difference between 40 and 45 was less than 1.6×10^{-6}. Therefore, a vertical grid size of 40 was chosen, which lead to a final grid size of 240×40.

The laboratory experiments resulted in temperature profiles for different Reynolds numbers, different heat inputs and different porosities. The results compared the local heat transfer coefficient with numerical data based on the bulk fluid temperature next to the wall and the inlet fluid temperature. The heat transfer coefficient based on the mean fluid temperature will also be discussed: both will be compared to the data obtained from Fluent™. The thermal dispersion of the different porosities will also be discussed. Finally, a correlation between the thermal modeling of a matrix heat exchanger based on the thermal modeling of porous medium will be evaluated.

Data was collected at various positions along the bottom, middle, and top of the porous medium section. The input velocities resulted in Reynolds numbers between 0.5 and 2.6 for the fine medium and between 0.5 and 3 for the coarse medium. The temperature profiles of the recorded data demonstrated that the temperatures rose as the fluid moved along the x-direction through the porous medium. The maximum temperatures were recorded at the bottom of the porous medium. The temperatures decreased the further the fluid was from the heat source. The temperature profiles can be seen in Fig. 6. In the following figures, the term 'num' defines the numerical model, while '*Re*' indicates data from the laboratory experiment, unless otherwise indicated.

The friction factor for the flow in the fine and coarse porosity was based on the equation [1]:

$$f = \frac{\varepsilon_m^3}{1-\varepsilon_m} \frac{\rho_f d_f}{3M^2} \frac{\Delta P}{L} \tag{30}$$

where, the mass flux, M, is $M = \rho_f u$ and

$$\varepsilon_m = \frac{\text{Volume}_{\text{total}} - \text{Volume}_{\text{porous}}}{\text{Volume}_{\text{total}}}$$

Jiang et al. [9] also presented a correlation for the friction factor as a function of Reynolds number:

$$f = \frac{36.4}{Re} + 0.45 \tag{31}$$

This value is valid for $Re < 2000$. The data collected in the laboratory experiments is plotted along with Eq. (31) in Fig. 7.

The heat transfer coefficient was evaluated based on the inlet temperature of the fluid. As mentioned in Section 10, the entrance effects were hard to capture with the laboratory experiment. As can be seen in Fig. 8 the difference at the entrance region is the greatest. The Fluent™ line represents the results for each of the same heat inputs. While the in-house numerical model's data more closely followed the trend of the laboratory experiments, the difference between the Fluent™ (LTE) results

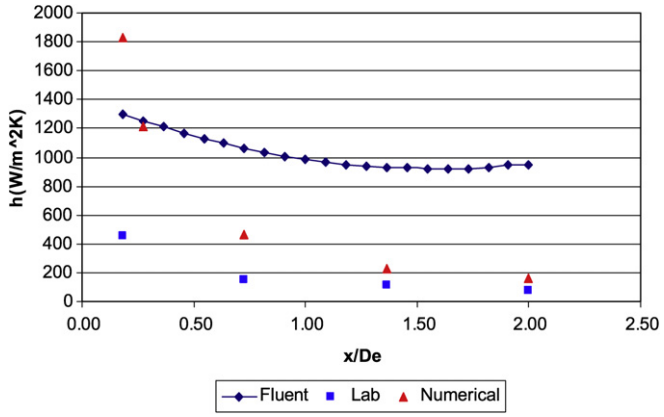

Fig. 8.

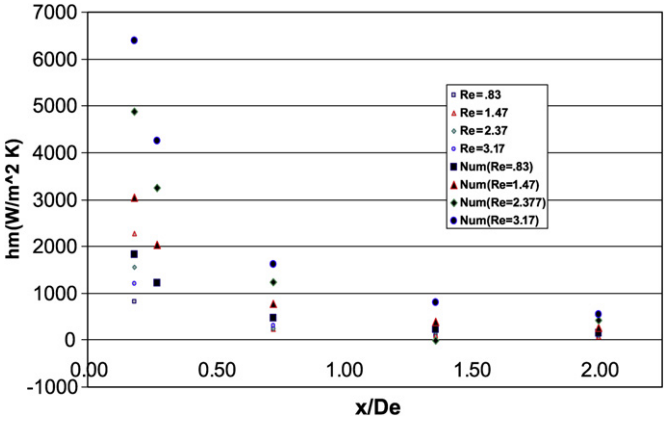

Fig. 9.

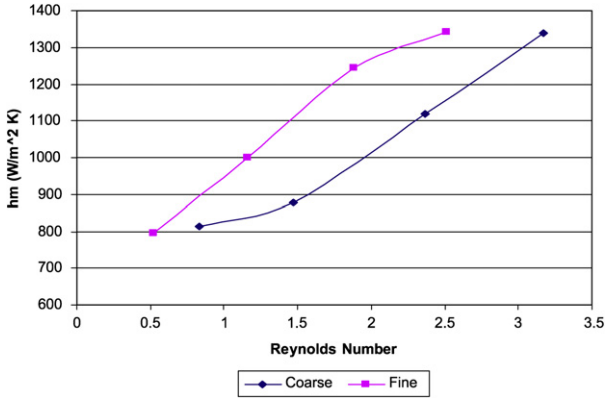

Fig. 10.

and the in-house numerical model (LTNE)/lab results are quite noticeable.

The overall heat transfer was found to increase as the *Re* increased initially within the porous medium, but was found to converge as the distance from the entrance increased: as can be seen in Fig. 9. Fig. 10 demonstrates how the Reynolds number affects the mean heat transfer coefficient based on the mean wall temperature.

Jiang et al. [9] found that the coefficient in the thermal dispersion conductivity model (Eq. (23)) decreased as the velocity increased. The amount of surface area in the porous medium

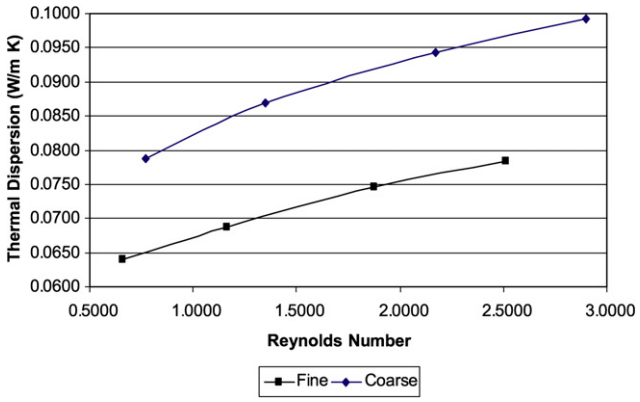

Fig. 11.

section is large: therefore the amount of water in contact with the porous surface is also large. The amount of heat transfer credited to the thermal dispersion can be seen in Fig. 11.

10. Application to the matrix heat exchanger

Research into the heat transfer coefficient of a perforated plate was conducted to determine a relationship between the Nusselt number and the Reynolds number taking into account the convection of the front, the back, and inside the perforation hole. It was found through various modeling done in Fluent™ that a correlation between the Nusselt number and the Reynolds was as follows:

$$Nu = 0.397Re^{0.652} \tag{32}$$

This correlation was based on the plate being a constant temperature. Sparrow et al. [1] did a similar experiment but based his results on the naphthalene sublimation technique. His experiment considered only the windward face of the perforated sheet.

The numerical porous model was modified to better represent the flow through a matrix heat exchanger. First, efficiency was assumed for the matrix heat exchanger. This efficiency was based on work done by Venkatarathnam [8]. Next $q_{\max}$ was determined by defining, $\dot{m}$, $T_{h,i}$ and $T_{c,i}$ using

$$q_{\max} = \dot{m}c_p(T_{h,i} - T_{c,i}) \tag{33}$$

Using (33) and the efficiency, q for the heat exchanger could be found.

$$q = \eta \cdot q_{\max} \tag{34}$$

The model was solved again for the temperature profiles. Different Reynolds numbers were investigated in order to determine the heat transfer characteristics. The average Nusselt number was then found and graphed. The resulting correlation between the matrix heat exchanger Nusselt number and the porous medium Nusselt number can be seen in Fig. 12. Fig. 12 also represents data of matrix heat exchanger research presented by Venkatarathnam and Sarangi [7] and Krishnakumar and Venkatarathnam [20] in which different researchers work is present: matrix heat exchangers with shifted holes and shifted slots from Subbotin's work, Venkatarathnam [8], Anashkin's

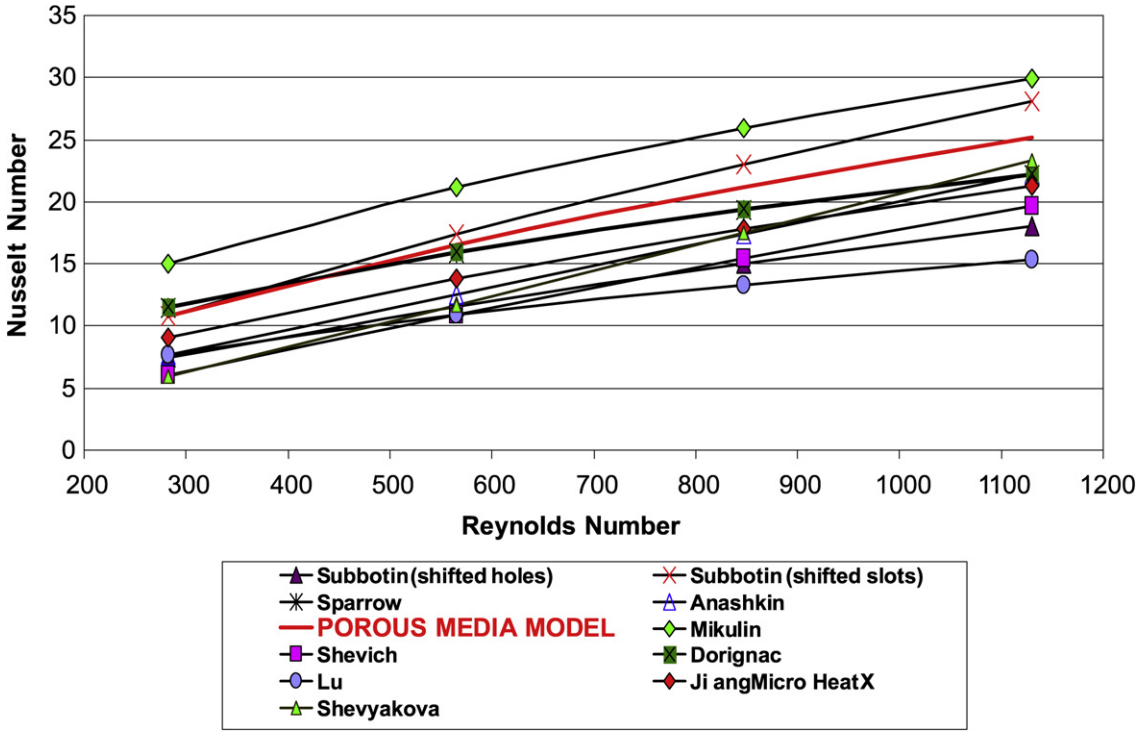

Fig. 12.

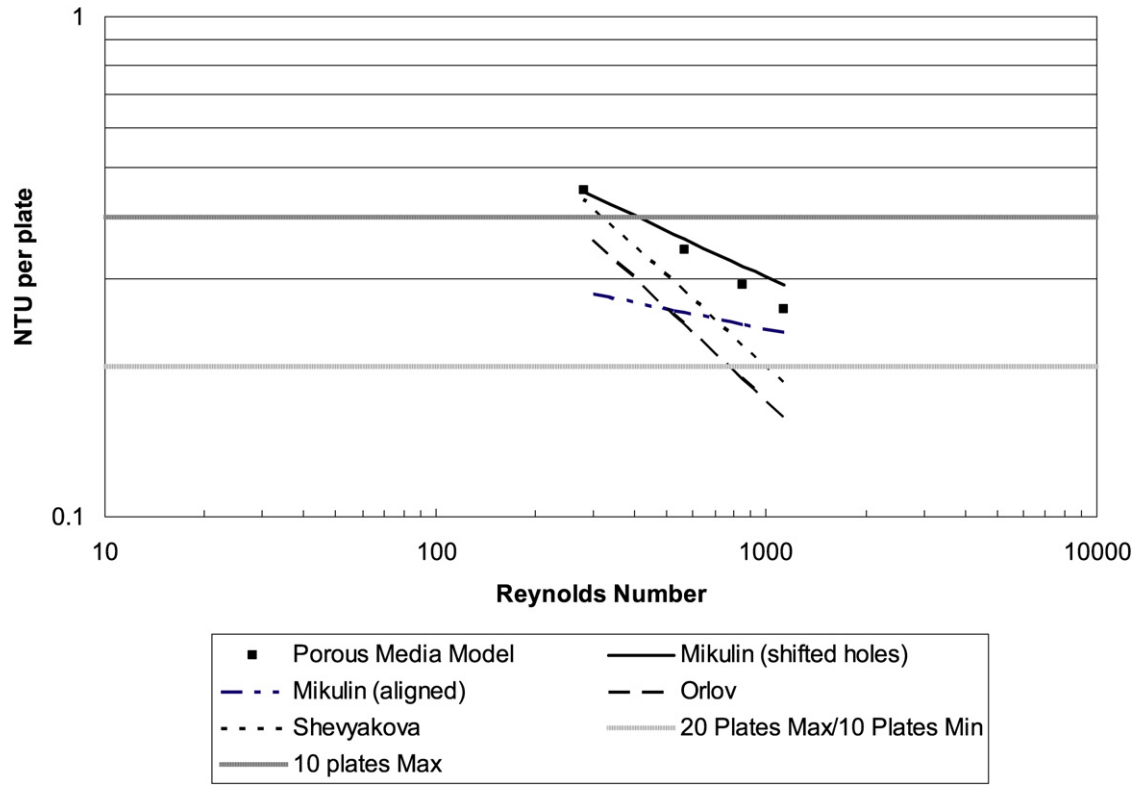

Fig. 13.

et al. [21] correlation, Mikulin and Shevich's early work at the N.E. Bauman technical Institute [8], Dorignac et al. [22], Lu et al. [23], Jiang et al. [10], Shevyakova and Orlov [24] and the Porous Medium Model from the current work.

The resulting equation for the Nusselt number using air as the working fluid:

$$Nu = 0.445 Pr^{1/3} Re^{0.607} \tag{35}$$

Or with $Pr = 0.707$

$$Nu = 0.396Re^{0.607} \tag{36}$$

The difference in the data for the Nusselt number correlations above can be attributed to the different test parameters each of the authors presented. For example, Dorignac's et al. [22] data was based on a perforated plate with large diameter perforations: on the order of 10 mm. While Jiang's et al. [10] micro-heat exchanger was 20 mm in length and had channels of dimensions 0.2 mm by 0.6 mm.

Krishnakumar and Venkatarathnam [20] made a number of transfer units, NTU, comparison in which they reported that the maximum slope (dimensionless temperature/dimensionless time) for a transient blow test at the exit of a matrix heat exchanger will occur when the total NTU is greater than 2. They showed that the total NTU must be less than 4 in order for conventional methods to be used in treating the heat exchanger. For 10 plates this gives a limit of NTU/plate of 0.2 and 0.4, while for 20 plates this yields a limit of 0.1 and 0.2. Fig. 13 uses the same assumptions as Krishnakumar and shows the variation of overall NTU/plate as a function of Reynolds number for various Nusselt number correlations. The points plotted are the results of the porous medium model, which lies within this range.

11. Conclusion

Through the use of a porous media model and assuming the thermal non-equilibrium a thermal model for heat transfer in a porous medium was developed and verified against laboratory data. This model was then modified to better assimilate a matrix heat exchanger. The results show favorable agreement between existing Nusselt correlations for heat transfer in a matrix heat exchanger as well as between NTU per plate correlations.

References

[1] E.M. Sparrow, M.C. Ortiz, Heat transfer coefficients for the upstream face of a perforated plate positioned normal to an oncoming flow, International Journal of Heat and Mass Transfer 25 (1) (1982) 127–135.

[2] H.H. Cho, R.J. Goldstein, M.Y. Jabbari, Experimental mass (heat) transfer in and near a circular hole in a flat plate, International Journal of Heat and Mass Transfer 40 (10) (1997) 2431–2443.

[3] L. Gong, T. Guo, J. Hu, T. Zhu, The effect of the geometric parameters of a perforated plate on its heat transfer characteristics, Cryogenics 36 (1996) 443–446.

[4] A.P. Brunger, K.G.T. Hollands, G.W.E. Van Decker, Heat-exchange relations for unglazed transpired solar collectors with circular holes on a square or triangular pitch, Solar Energy 71 (1) (2001) 33–45.

[5] U. Imke, Porous media simplified simulation of single- and two-phase flow heat transfer in micro-channel heat exchangers, Chemical Engineering Journal 101 (2004) 295–302.

[6] K. Boomsma, D. Poulikakos, F. Zwick, Metal foams as compact high performance heat exchangers, Mechanics of Materials 35 (2003) 1161–1176.

[7] G. Venkatarathnam, S. Sarangi, Matrix heat exchangers and their application in cryogenic systems, Cryogenics 30 (11) (1990) 909–918.

[8] G. Venkatarathnam, Effectiveness–NTU relationship in perforated plate matrix heat exchangers, Cryogenics 30 (4) (1996) 235–241.

[9] P.-X. Jiang, Z.-P. Ren, Numerical investigation of forced convection heat transfer in porous media using thermal non-equilibrium model, International Journal of Heat and Fluid Flow 22 (2001) 102–110.

[10] P.-X. Jiang, M.-H. Fan, G.-S. Shi, Z.-P. Ren, Thermal hydraulic performance of small scale micro-channel and porous-media heat-exchangers, International Journal of Heat and Mass Transfer 44 (2001) 1039–1051.

[11] K. Vafai, S.J. Kim, On the limitations of the Brinkman–Forchheimer-extended Darcy equation, International Journal Heat and Fluid Flow 16 (1995) 11–15.

[12] B. Pavel, I. Mohamad, A. Abdulmajeed, An experimental and numerical study on heat transfer enhancement for gas heat exchangers fitted with porous media, International Journal of Heat and Mass Transfer 47 (2004) 4939–4952.

[13] B. Alazmi, K. Vafai, Constant wall heat flux boundary conditions in porous media under local thermal non-equilibrium conditions, International Journal of Heat and Mass Transfer 45 (2002) 3071–3087.

[14] H.Y. Zhang, X.Y. Huang, Volumetric heat transfer coefficients in solid–fluid porous media; closure problem, thermal analysis and model improvement with fluid flow, International Journal of Heat and Mass Transfer 43 (2000) 3417–3432.

[15] T.-M. Jeng, S.-C. Tzeng, Y.-H. Hung, An analytical study of local thermal equilibrium in porous heat sinks using fin theory, International Journal of Heat and Mass Transfer 49 (2006) 1907–1914.

[16] S. Whitaker, The Method of Volume Averaging, vol. 13, Kluwer Academic Publishers, Dordrecht, 1999, p. 89.

[17] S.A. Khashan, A.M. Al-Amiri, I. Pop, Numerical simulation of natural convection heat transfer in a porous cavity heated from below using a non-Darcian and thermal non-equilibrium model, International Journal of Heat and Mass Transfer 49 (2006) 1039–1049.

[18] M.M. Gupta, J.C. Kalita, A new paradigm for solving Navier–Stokes equations: Streamfunction-vorticity formulation, Journal of Computational Physics 207 (2005) 52–68.

[19] F.P. Icorpra, D.P. DeWitt, Fundamentals of Heat and Mass Transfer, third ed., John Wiley & Sons, Inc., New York, 1990.

[20] K. Krishnamkumar, G. Venkatarathnam, Transient testing of perforated plate matrix heat exchanger, Cryogenics 43 (2003) 101–109.

[21] O.P. Anashkin, V.E. Keilin, V.M. Patrikeev, Compact high efficiency perforated plate heat exchangers, Cryogenics (July 1976) 437–439.

[22] E. Dorignac, J.J. Vullierme, M. Broussely, C. Foulon, M. Mokkadem, Experimental heat transfer on the windward surface of a perforated flat plate, International Journal of Thermal Sciences 44 (2005) 885–893.

[23] W. Lu, C.Y. Zhao, S.A. Tassou, Thermal analysis on metal-foam filled heat exchangers. Part I: metal-foam filled pipes, International Journal of Heat and Mass Transfer (2006), in press.

[24] S.A. Shevyakova, V.K. Orlov, Study of hydraulic resistance and heat transfer in perforated-plate heat exchangers, Inzhenerno-Fizicheskii Zhurnal 45 (1) (1983) 32–36. Translated by Balashinsk Scientific-Industrial Association of Cryogenic Machine Construction, 1984.